

Periodically bursting edge states in plane Poiseuille flow

Stefan Zammert¹‡ and Bruno Eckhardt^{1,2}

¹ Fachbereich Physik, Philipps-Universität Marburg, Germany

² J.M. Burgerscentrum, Delft University of Technology, Mekelweg 2, 2628 CD Delft, The Netherlands

E-mail: Stefan.Zammert@physik.uni-marburg.de

Abstract. We investigate the laminar-turbulent boundary in plane Poiseuille flow by the method of edge tracking. In short and narrow computational domains we find for a wide range of Reynolds numbers that all states in the boundary converge to a periodic orbit with a period of the order of 10^3 time units. The attracting states in these small domains are periodically extended in the spanwise and streamwise direction, but always localized to one side of the channel in the normal direction. In wider domains the edge states are localised in the spanwise direction as well. The periodic motion found in the small domains then induces a large variety of dynamical activity that is similar to one found in the asymptotic suction boundary layer.

Keywords: Fluid dynamics, Bifurcations, Coherent structures, Transition

1. Introduction

In shear flows such as plane Couette, plane Poiseuille, duct or pipe flow it is possible to observe sustained turbulence for Reynolds numbers where the laminar state is still stable against infinitesimal perturbations. These flows, therefore, show a coexistence of two dynamically distinct states, a stable laminar flow, and a dynamically active, turbulent state. In the simplest cases each state is attractive, in which case the boundary between them is the boundary separating the two basins of attraction. The transient behaviour of the chaotic states in shear flows (Hof et al. 2006) requires an extension of the concept of a basin boundary to cover transient cases as well. It was given in Skufca et al. (2006) (see also Schneider et al. (2007) and Vollmer et al. (2009)) and uses the lifetime of perturbations as indicator. Increasing the amplitude of the perturbation one notes a clear transition from a region in which the lifetime varies smoothly and the trajectories return to the laminar profile, to a region with irregularly fluctuating lifetimes where the perturbations initially approach a state that has all the characteristics of a turbulent state, before eventually returning to the laminar state. Points on the boundary between the two regions are on the “edge of chaos”, and when tracking their time evolution one notes that they approach a state that is a relative attractor within this boundary, the so-called edge state (Skufca et al. 2006).

The significance of this method lies in the ease with which it provides access to exact coherent states. Exact coherent states play a major role in our current understanding of the transition to turbulence in shear flows and they can also contribute to the understanding of the turbulent dynamics (Eckhardt et al. 2007, Kawahara et al. 2012). They range from the stationary states first identified in plane Couette flow (Nagata 1990, Clever & Busse 1997, Waleffe 1998) to the travelling waves and relative periodic orbits in pipe flow (Faisst & Eckhardt 2003, Wedin & Kerswell 2004, Eckhardt et al. 2008, Pringle & Kerswell 2007, Duguet et al. 2008, Mellibovsky & Eckhardt 2012), in duct flow (Uhlmann et al. 2010) and in plane Couette and Poiseuille flow (Waleffe 1998, Kawahara & Kida 2001, Gibson et al. 2009, Itano & Generalis 2009, Gibson & Brand 2014, Nagata & Deguchi 2013). Edge tracking is a robust method for identifying coherent structures: whereas almost all other methods require a good guess of initial conditions, edge tracking will invariably converge to an invariant state for just about any initial condition.

The edge states themselves are important for the delineation of the stable-unstable border, and for the identification of minimal or most dangerous disturbances that trigger turbulence (Cherubini et al. 2012). In addition, they are also indicative of the possible behaviour of the other states around which turbulence forms. Specifically, it has been possible to track a few of these states to their saddle-node bifurcation point and to follow the corresponding upper branch states, and thereby to gain information about the states underlying the turbulent dynamics (Kreilos & Eckhardt 2012, Avila et al. 2013).

States on the boundary between laminar and turbulent behaviour were first identified in small periodic domains by Toh & Itano (2003) (see also Toh & Itano 1999, Itano & Toh 2001), followed by independent studies of low-dimensional models

(Skufca et al. 2006), of pipe flow (Schneider et al. 2007) and of plane Couette flow (Schneider et al. 2008). For extended domains it was shown by several authors that the attracting objects in the edge of chaos are localised states (Duguet et al. 2009, Schneider, Marinc & Eckhardt 2010, Mellibovsky et al. 2009, Avila et al. 2013). The connection between narrow and wide domains was discussed in the context of snaking bifurcations (Schneider, Gibson & Burke 2010) and long-wavelength instabilities (Melnikov et al. 2013). Spatially extended flows, such as boundary layers, can also be approached with this method (Cherubini et al. 2011, Duguet et al. 2012), and states intermediate between laminar and turbulent can be identified. The spatial growth of the boundary layer can be avoided by applying a cross flow that maintains the width of the layer, as in the case of the asymptotic suction boundary layer (ASBL). The edge states for ASBL in narrow domains were identified in (Kreilos et al. 2013), and further studies revealed a rich variety of localised but dynamically active states (Khapko et al. 2013a, Khapko et al. 2013b). This dynamical activity is compatible with the possibility that the edge states are not simple attractors but that they can be more complicated and perhaps even chaotic (Schneider et al. 2007, Vollmer et al. 2009).

In this paper we study plane Poiseuille flow (PPF), the pressure driven flow between parallel walls. To define a Reynolds number, $Re = U_0 d / \nu$, for this flow we use half the distance between the plates d and the maximum velocity U_0 of the laminar profile in the center of the channel. PPF shares many features with the other shear flows, but differs in the presence of a linear instability of the laminar flow at a Reynolds number of $Re = 5772$ (Orszag 1971). The linear instability of the laminar flow creates a two-dimensional travelling wave that can be continued to lower Re . The secondary instabilities of this wave create 3-dimensional exact solutions studied e.g. by Ehrenstein & Koch (1991). However, these solutions are not reached with the initial conditions we use in our edge tracking.

Below the critical Reynolds number for the linear instability, PPF shows a coexistence of transient but long living turbulence and a linearly stable laminar profile, so that the technique of edge tracking can be applied and the invariant states in the edge can be identified. For a small computational domain and at one fixed Reynolds number, Toh & Itano (2003) found that the edge state is a periodic orbit. We will here confirm their finding and extend it to wider domains and other Reynolds numbers, where a rich bifurcation scenario and a large variety of other edge states can be identified. In addition, we will show that for wide and not too long computational domains the edge states are spanwise localised orbits with intriguing spanwise dynamics.

As in other studies, we rely for our numerical simulations on the code *Channelflow*, developed and maintained by Gibson (2012). The code uses a spectral method to simulate a doubly periodic domain with a streamwise extent L_x , a spanwise extent L_z and a wall-normal extent of $L_y = 2$. It uses a decomposition of the full flow field $\tilde{\mathbf{u}}$ into the laminar flow $\mathbf{U} = (U(y), 0, 0)$ with $U(y) = 1 - y^2$ and the deviations \mathbf{u} . The flow field $\mathbf{u} = (u, v, w)$ is expanded in N_x and N_z Fourier modes in the streamwise and spanwise direction and in N_y Chebychev modes in the wall-normal direction. In our

simulation these numbers reach up to $32 \times 65 \times 96$ in the largest domains. The code imposes periodic boundary conditions in streamwise (x) and spanwise (z) directions and no-slip boundary conditions at the walls. In all calculations we impose constant mass flux. For further details on the code we refer to the `channelflow` manual. The edge tracking algorithm is discussed in several papers, see e.g. Itano & Toh (2001), Toh & Itano (2003), Skufca et al. (2006) or Dijkstra et al. (2014).

The outline of the paper is as follows. In section 2, we discuss the edge states in short and narrow domains. In section 3, we discuss the spanwise localised states and their dynamics, and in section 4 we end with a summary and an outlook.

2. Edge states in short and narrow domains

The first edge tracking calculations in PPF were carried out by Toh & Itano (2003). The domain they used was quite small and had streamwise and spanwise widths of π and 0.4π , respectively. Their edge trajectories are characterised by long intervals of nearly constant energy with only small variations in the flow structure and sudden bursting events that separate these intervals. In order to reproduce their results, we used the same periodic domain and a spectral resolution of $N_x \times N_y \times N_z = 32 \times 65 \times 32$. Starting from arbitrary turbulent fields as initial conditions for edge tracking, we obtain edge states that show the same features as the ones obtained by Toh & Itano (2003) using especially shaped initial conditions.

One example for an edge tracking is shown in figure 1 for the Toh-Itano domain size and at $Re = 3000$. The state is characterised by its energy content,

$$E(\mathbf{u}) = \frac{1}{L_x L_y L_z} \int \mathbf{u}^2 dx dy dz, \quad (1)$$

shown along the ordinate. The figure also illustrates how the genuine edge trajectory is approximated by trajectories on the laminar (low energy) and on the turbulent (high energy) side of the edge. As a criterion for becoming turbulent or laminar we use upper and lower thresholds for the energy. One notes that the bursts are spaced in time by about 1000 units (d/U_0). Given the small size of the domain and consequently the short time of 4.7 time units that a structure needs to traverse the domain at mean speed $\bar{u}/U_0 = 2/3$, this is a very long time. The time on the abscissa is counted from the start of the edge tracking, and indicates that it took several thousand time units to converge to this state, referred to as PO_1 in the following. We observed a very slow convergence to the edge state for all trajectories studied.

Because of the regularity of the edge trajectory, Toh & Itano (2003) speculate that the trajectory is attracted by a limit cycle or heteroclinic connection. Visualisations of the flow in the spanwise wall-normal plane at $x = 0$ are given in figure 2 for the times marked by the black circles in 1. They show that the state is indeed periodic, but with a period that is twice the one that one would read off from the energy vs. time diagram. As is evident from the figure, the state consists of a pair of streaks located near one wall that changes only slightly over a long time interval, but then splits into

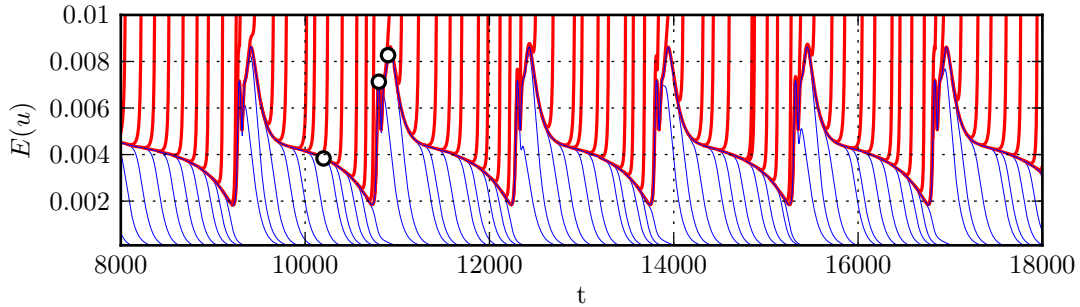


Figure 1. Edge tracking at $Re = 3000$ in a domain with size $L_x = \pi$ and $L_z = 0.4\pi$. For each refinement step the energies of the final turbulent and laminar trajectories are shown. The flow in the streamwise wall-normal plane is shown in figure 2 for the times marked by the black circles.

two pairs of streaks, and reforms after a short time interval as a state with a single pair of streaks that is similar to the initial one except for a shift in the spanwise direction by half a domain width. Therefore, after one period in energy one obtains the initial flow structure but shifted by half the domain width. The evolution of the streak during one period is shown in figure 3(a), where the time-variation of the streamwise velocity at fixed x -coordinate and at a distance of 0.223 from the lower plate is shown. In addition, in figure 3(b) the full energy $E(\mathbf{u})$ and the crossflow energy,

$$E_{cf}(\mathbf{u}) = \frac{1}{L_x L_y L_z} \int (v^2 + w^2) dx dy dz,$$

are shown as a function of time. The cross-flow energy is a more reliable indicator of persistent dynamics since the flow will relaminarize if its value is too low. In addition, we show the instantaneous advection velocity c_x of the structure as defined in Kreilos & Eckhardt (2013) in figure 3(c). The instantaneous velocity varies very little over a long time interval, as is typical for trajectories close to a travelling wave. Shortly before the bursts that displace the streaks, c_x is reduced drastically, but recovers to the previous values again once the new position is reached. The periodic orbit shows many of the features described in the self-sustaining process (Waleffe 1997). During the quiet phases the state consists of a pair of streaks that decay slowly, resulting in a slow decrease of total energy. At a certain point in time the streaks undergo an instability, new vortices form and the crossflow energy content increases dramatically. The vortices then drive strong streaks that undergo instabilities that nucleate further streaks and the cycle starts again.

The periodic edge state is surprisingly similar to the one studied in detail by Kreilos et al. (2013) in the asymptotic suction boundary layer (ASBL). The similarity of the two states can be explained by the fact that the base profile of the ASBL close to the wall is similar to one half of the Poiseuille profile, from the wall to the midplane. More specifically, the first two derivatives of the dimensionless profiles of ASBL ($U(y) = 1 - e^{-y}$) and PPF ($U(y) = 1 - y^2$) at the position of the lower wall ($y = 0$ for ASBL and $y = -1$ for PPF) are equal up to a factor of two. For the ASBL the

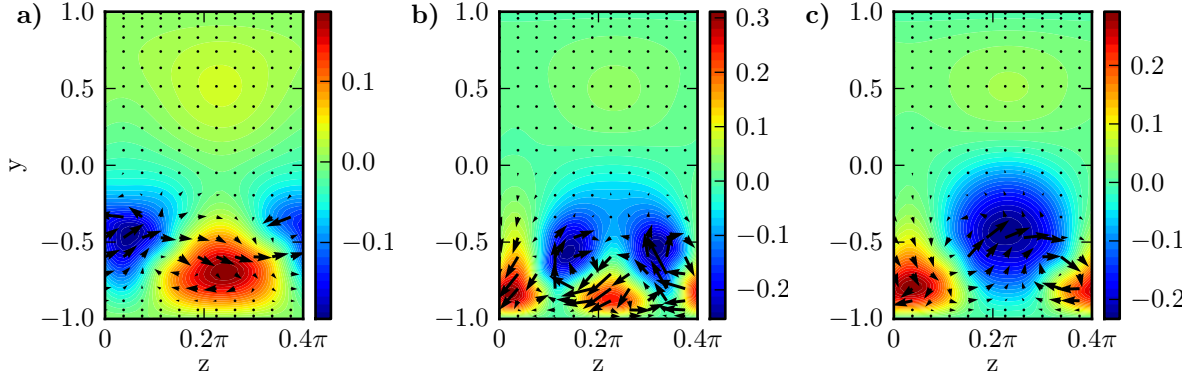


Figure 2. Flow in the spanwise wall-normal plane at $x = 0$ for the times marked by the black circles in figure 1. The streamwise velocity (deviation from the laminar profile) is colour coded (color online) and the velocity in the plane is visualised by the arrows.

periodic edge state is created in a SNIPER bifurcation (Kreilos et al. 2013, Tuckerman & Barkley 1988, Strogatz 1994) with increasing suction velocity. During the quiet phases the flow structure in the lower part of the channel is similar to the lower branch of the well-studied NBC-solution (Nagata 1990, Clever & Busse 1997) that is an edge state in plane Couette flow. The similarity becomes evident by comparing the visualisation of the NBC-state of Melnikov et al. (2013) to the lower half of the visualisation of the flow during the quiet phase shown in figure 2(a).

The period of the state is too long to converge it with a Newton method, so we use edge tracking to continue the orbit in Reynolds number. A flow field of the orbit at one Reynolds number is used as a starting point for edge tracking at a neighbouring Reynolds number. To verify that we are still tracking the relevant edge states, we performed independent edge trackings starting from random initial conditions for isolated values of Re . We were able to trace edge states in Reynolds numbers to about 2100. They are similar to PO_1 in that all edge trajectories show bursts in energy. However, there are differences in detail, and for some Re the sequence of bursts is not periodic but chaotic.

In figure 4(a) we show the variation of the edge state with Re by plotting the time between two bursts along an edge trajectory. For values of Re where the attracting edge state is periodic, the distance between two bursts becomes constant after an initial transient, resulting in a single square entry in figure 4. For period doubled states there are two different time lapses between bursts, resulting in two squares in the figure. For Reynolds numbers where even after a long transient time (about 20000 time steps) the time between two bursts varies randomly, we plot the inter-burst times using small dots; they are then spread out over an interval of inter-burst periods. As a second indicator we show in figure 4(b) the maximum energy during the bursts.

Orbits that share with PO_1 the property that they shift by half a wavelength in spanwise direction during one period in energy exist for various values of Re . Such orbits are shown in figure 4 using blue squares as symbols. They undergo various bifurcations

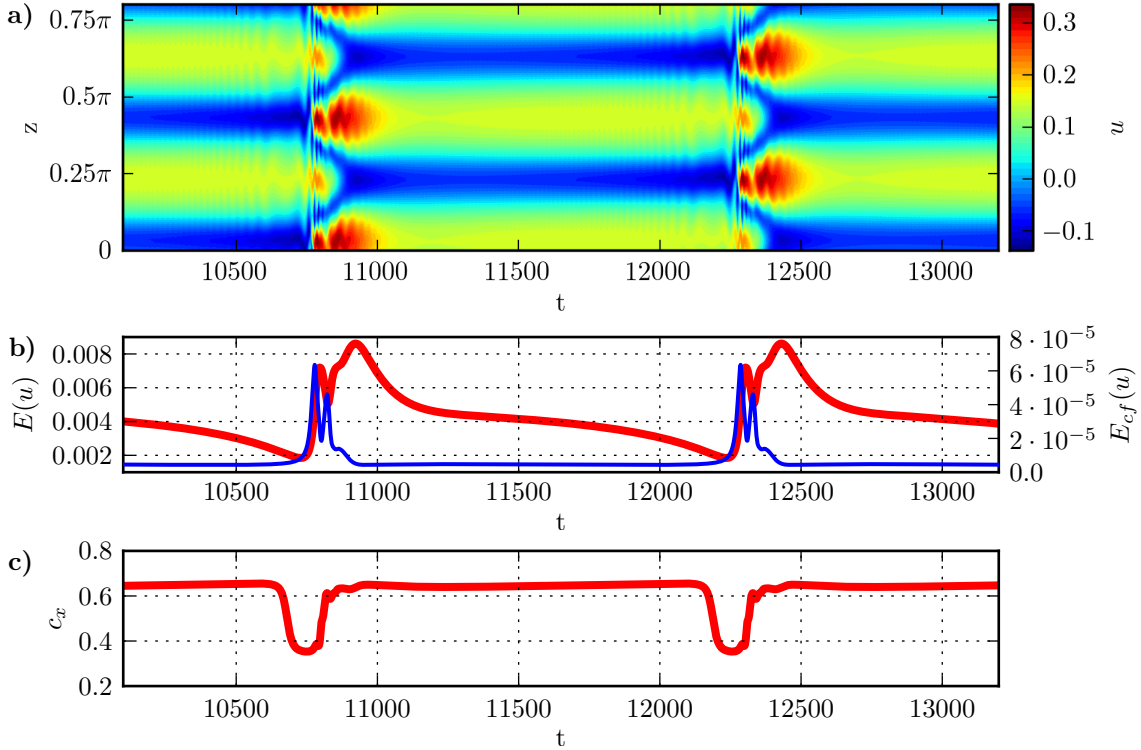


Figure 3. Time evolution of the periodic edge state (PO_1) shown in figure 1. Panel (a) shows the streamwise velocity at position $x = 0$ in a distance of 0.223 from the lower wall $vs.$ time and reveals the spanwise dislocation by half a domain width. Panel (b) shows the total (thick red line) and cross-flow energy (thin blue line) for the same time interval and the massive increase during the burst events. Panel (c) shows the downstream advection velocity c_x (determined as explained in Kreilos et al. (2013)) of the structures; it drops noticeably during the bursts.

with increasing Re . One example is shown in the inset in figure 4(b), where a period-2 state is created in a forward bifurcation at $Re \approx 2950$ and disappears again in an inverse pitchfork bifurcation at $Re \approx 2987$.

Another set of edge states, labelled PO_2 , is found for $3200 < Re < 3300$ (green circles in figure 4). The states have relatively low periods between 400 and 500 time units and differ from PO_1 in that the structures do not shift by half a wavelength in spanwise direction over one period in energy. Specifically, after one period in energy the flow field equals the original one except for a spanwise reflection ($s_z : [u, v, w](x, y, z) = [u, v, -w](x, y, -z)$). The dynamics of the PO_2 -state is visualised in figure 5. It undergoes a Neimark-Sacker bifurcation close to $Re = 3300$, and then further bifurcations as Re increases until it finally disappears close to $Re = 3600$.

Yet another periodic orbit, PO_3 , is found for Re around 3800 (red triangles in figure 4). It differs from the above orbits in the displacement following the burst, which is only $0.385L_z$ (see figure 6). It seems to exist in a small range in Re only. The deviation of the shift from half a domain width is a precursor to the behaviour in wider domains, where the sideways displacement becomes a consequence of the intrinsic dynamics and

is not correlated with the width of the domain (a phenomenon also seen in the ASBL by Khapko et al. (2013a, 2013b)).

In order to demonstrate the periodicity of the orbits, we consider the orbit PO_2 at $Re = 3250$. In figure 7 we show the energy of the difference between the initial velocity field and a symmetry related one at a later time, $u(t_0) - S(u(t_0 + t))$. The symmetry operation S consists of a reflection in spanwise direction (at the axis shown in figure 5) and the streamwise shift that gives the minimal difference for a given value of t . The time between the two peaks with minimal energy is 934.05 and corresponds to two periods T in energy. Therefore, for $Re = 3250$ the period in energy of PO_2 is approximately $T = 467.025$. After applying the appropriate symmetry operations the energy of the difference of two flow fields after a time T is of order 10^{-8} , demonstrating that the orbit is closed. The streamwise shift for which this minimal error is achieved is $0.628L_x$. Similarly, we obtain an energy difference for PO_1 at $Re = 3000$ of $2 \cdot 10^{-7}$ for $T = 1508$ and for PO_3 at $Re = 3800$ of $1 \cdot 10^{-7}$ for $T = 1333.5$. The streamwise and spanwise shifts that minimize the error are $0.956L_x$ and $0.5L_z$ for PO_1 and $0.698L_x$ and $0.385L_z$ for PO_3 .

In addition to the three orbits PO_1 , PO_2 , and PO_3 highlighted above there are also more complicated relative attractors in the edge. In particular, in the region between $Re = 3000$ and $Re = 3100$, many different states can be found. Among them are period doubled states, e.g. near $Re = 2960$ and 3095 . States with higher periods exist as well: for instance, at $Re = 3090$ the relative attractor shows six different maxima in energy and hence corresponds to a period 6 state. For $Re = 3035$ the edge trajectories are chaotic but show intermittent behaviour: the trajectories stay near a periodic state with essentially constant inter-burst period for several 1000 time units before they enter a chaotic phase. For the slightly smaller Reynolds number of $Re = 3030$ the attracting state in the edge is chaotic without any intermittency, but the flow structure and the dynamics is quite similar to the periodic orbits at slightly higher Re , as is evident from the visualisation of the edge trajectory shown in figure 8.

3. Spanwise localised edge states

The fact that the dynamics of the plane Poiseuille edge state in small periodic computational domains looks very much like that of the edge states in the ASBL suggests a similar behaviour in wider domains. Specifically, we can expect that the states become localised, and that the periodic sideways jumps become periodic or aperiodic translations in the spanwise direction (Khapko et al. 2013a, Khapko et al. 2013b).

Since for PPF the domain width where the bursting periodic orbits exists is by a factor of 5 smaller than the domain where the non-localised edge state in ASBL exists ($L_z = 2\pi$) the width that is necessary for localised states might also be significantly smaller. To check this, we ran edge tracking in a periodic domain with a width of 1.5π and 2π in the streamwise and spanwise direction, respectively, and a resolution of $N_x \times N_y \times N_z = 32 \times 65 \times 96$. The edge trajectories are attracted by a periodic state that

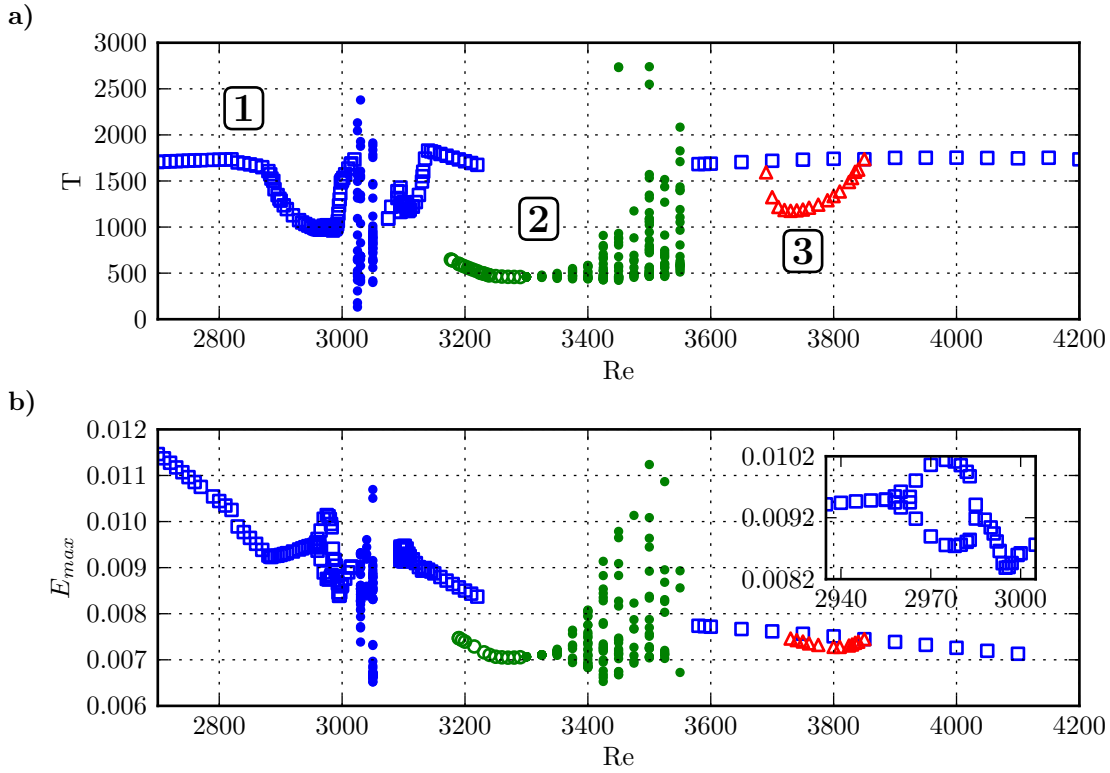


Figure 4. Bifurcation diagram for the edge states as a function of Re . The labels 1, 2 and 3 indicate where the periodic orbits PO_1 , PO_2 , and PO_3 are located. Panel (a) shows the times between two burst. If the edge has been identified as a periodic state, the values are shown as large symbols, if it is aperiodic small dots are shown. Panel (b) shows the maximum energy during the burst for the states shown in (a). The inset shows a small window where, with increasing Re the state first undergoes a period-doubling, which then is reversed.

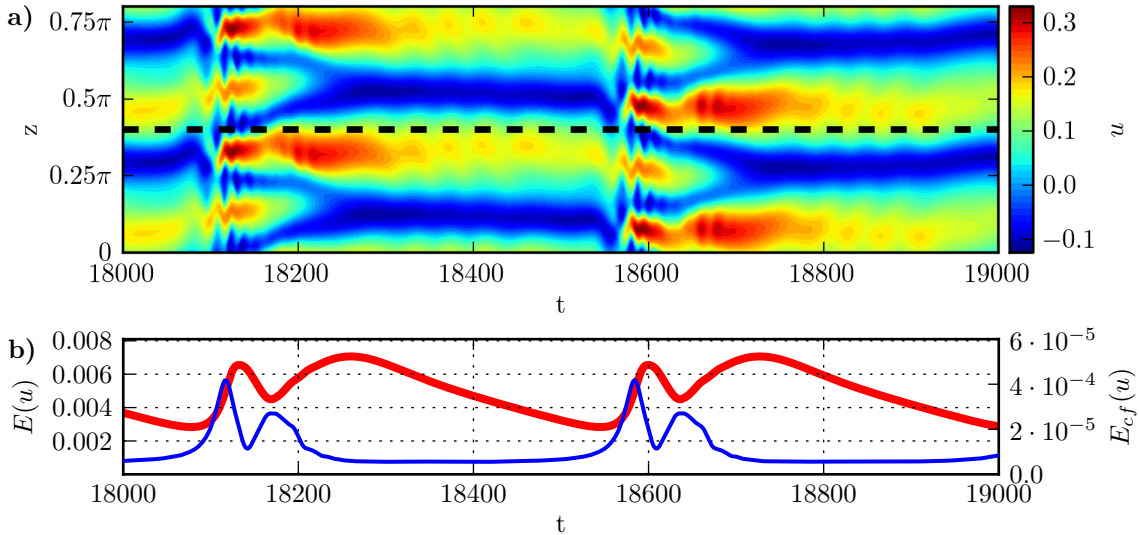


Figure 5. Space-time dynamics for the periodic orbit PO_2 . The visualisations are the same as in figure 3. One can clearly see that the state recurs with a reflection at the dashed line. The Reynolds number is 3250.

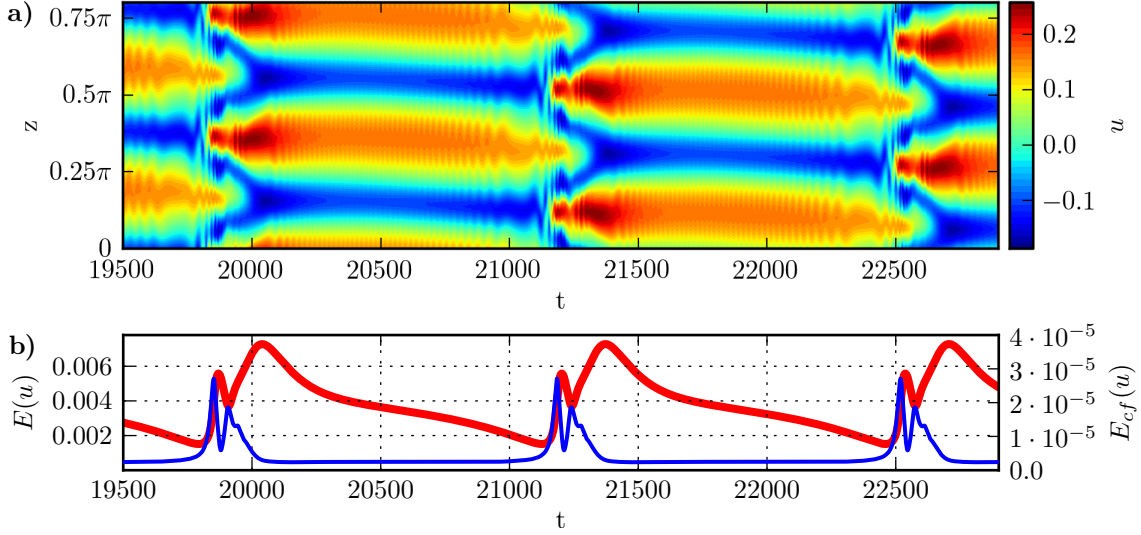


Figure 6. Space-time dynamics for the periodic orbit PO_3 . The visualisations are the same as in figure 3. This time the displacement in the spanwise direction is $0.385L_z$. The Reynolds number is 3800.

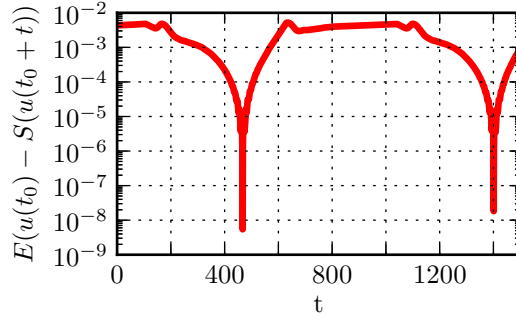


Figure 7. Energy of the difference flow field $u(t_0) - S(u(t_0 + t))$ as a function of t for $t_0 = 17964$. The symmetry operation S consists of a reflection in spanwise direction s_z (at the axis shown in figure 5) and the streamwise shift that gives the minimal difference for the value of t . The energy of the difference field has minima for $t = T$ and $t = 3T$.

is quite similar to the orbits in the small periodic domains and is in addition localised in the spanwise direction. The flow visualisation in figure 9 show that the state consists of a strong high-speed streak and two low-speed streaks of unequal strength to the left and to the right of the high speed streak.

A space-time plot of the dynamics obtained in the same manner as in the previous section is shown in figure 10 together with the time variation of the total and the crossflow energy. The visualisation reveals that the state shifts by approximately 0.4π in spanwise direction in each period and that the direction of the shift is always the same. In the following we will refer to this state as $PO_{E,R}$. By reflection symmetry, there also exists a state $PO_{E,L}$ that always shifts in the opposite direction. The orbits

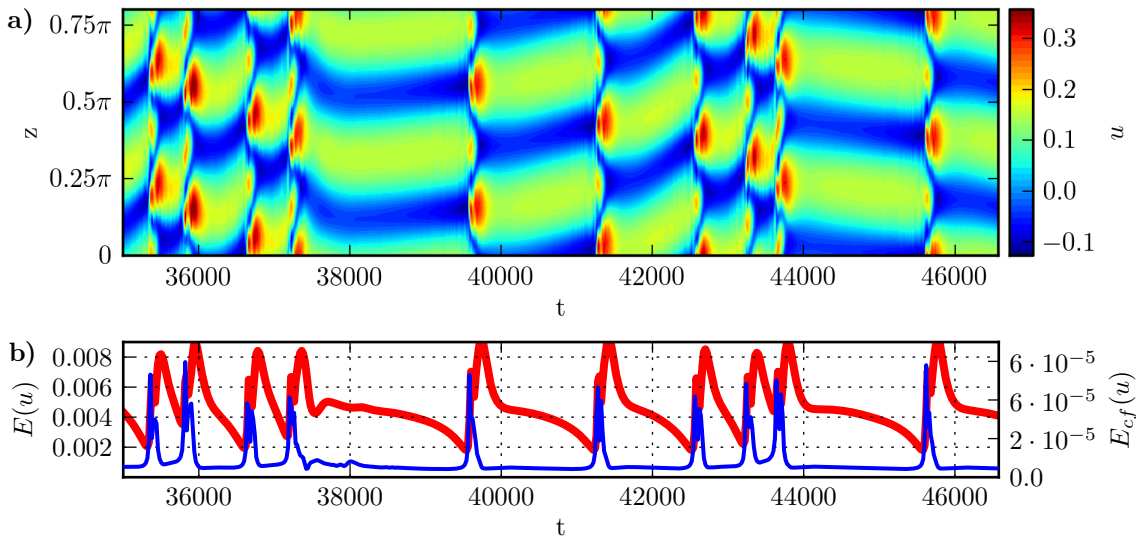


Figure 8. Space-time dynamics for a chaotic edge state at $Re = 3030$. The visualisations are the same as in figure 3.

are reminiscent of the L- and R-states found by Khapko et al. (2013a) in the asymptotic suction boundary layer (ASBL).

A good measure that reveals the spanwise localisation is the energy density integrated over the downstream and normal range, but resolved along the spanwise coordinate z . The total and the cross flow energy density *vs.* z are shown in figure 11 for $t = 16700$. The total energy density varies by about two orders of magnitude and the density of the crossflow energy by three orders of magnitude, indicating that even in this relatively narrow domain the state is already strongly localised in spanwise direction.

Since the periodic orbits in these domains as well as the ones in the narrower domains have very long periods, it is not possible to track the orbits sufficiently accurately for a direct stability analysis through the calculation of eigenvalues. Instead, we use first return maps to investigate the stability. We collect maxima of the \mathcal{L}^2 -norm, $\mathcal{L}^2(\mathbf{u}) = \sqrt{E(\mathbf{u})}$, and then plot the $i + 1$ -th maximum vs. the i -th maximum, as shown in figure 11(b). The slope β of the points close to the diagonal reveals the stability. For $|\beta| < 1$ the orbit is stable (Khapko et al. 2013b). Indeed, for $PO_{E,R}$ the slope is about -0.63 , so that we can conclude that it is a stable attractor within the edge.

As in the case of ASBL there are also states with regular or irregular sequences of left and right displacements. As an example, we show in figure 12 an LR-state in a domain with a streamwise length of 1.15π and a spanwise width of 2π . We will refer to this state as $PO_{E,LR}$. However, in contrast to the ASBL, where the R- and LR- state are both of codimension-one for particular values of L_x , this does not seem to be the case for $PO_{E,R}$ and $PO_{E,LR}$.

The presence of two walls seems to have a negligible effect on the qualitative dynamics. The states are located near one of the walls and there are also some weaker

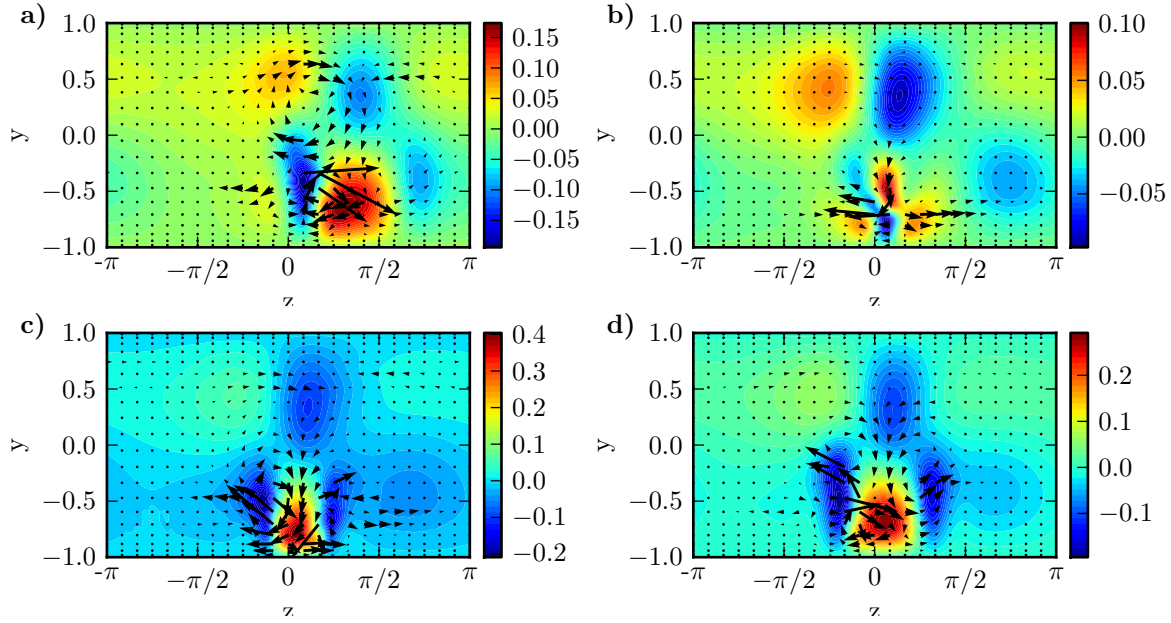


Figure 9. Flow in the spanwise wall-normal plane at $x = 0$ for the times marked by the black circles in figure 10. The streamwise velocity (deviation from the laminar profile) is colour coded and the velocity in the plane is indicated by the arrows. The Reynolds number is 3000 and the length and width of the domain are 1.5π and 2π , respectively.

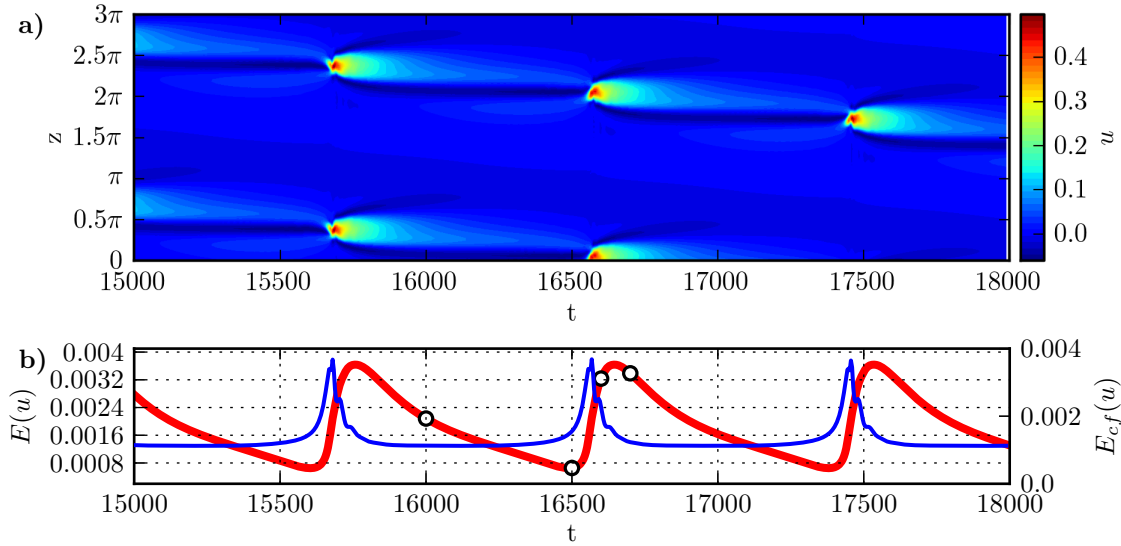


Figure 10. Localised state in a wide computational domain. The visualisations are the same as in figure 3, except that the velocity is recorded at $y = -0.858$. The flow in the streamwise wall-normal plane is shown in figure 9 for the times marked by the black circles.

streaks on the opposite side of the channel, see figure 9, but the effect on the spanwise dynamics is small.

When the domain length is varied the orbits $PO_{E,R}$ and $PO_{E,LR}$ undergo

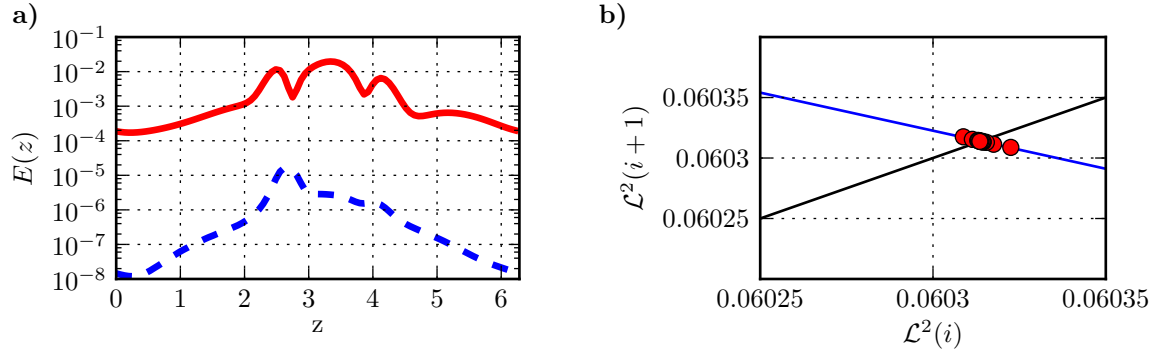


Figure 11. Spanwise localised state $PO_{E,R}$ and its stability analysis by the method of returns. (a) Total (solid red line) and cross flow (dashed blue line) energy density *vs.* spanwise coordinate z for the periodic orbit at $t = 16700$. (b) First return map of the \mathcal{L}^2 -norm at its maximum value.

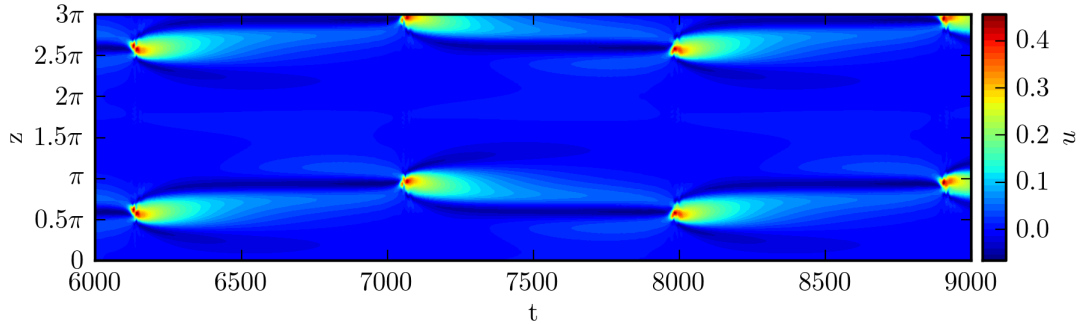


Figure 12. Space-time representation of the periodic orbit $PO_{E,LR}$. Shown is the streamwise velocity at $y = -0.858$ and $x = 0$ versus time. The Reynolds number is 3000 and the length and width of the domain are 1.15π and 2π , respectively.

bifurcations that lead to more complex periodic states and also chaotic ones. The continuation of the spanwise localised states in the domain length using edge tracking shows that $PO_{E,R}$ or $PO_{E,LR}$ or states that are bifurcations of these states with a more complex time dependence are attracting states only for $L_x < 1.7\pi$. For longer domains edge trajectories show periodic behaviour that is similar to the one of $PO_{E,R}$ or $PO_{E,LR}$ only transiently.

4. Conclusions and Outlook

The study of edge states in plane Poiseuille flow has revealed a rather rich variety of states. Some of the findings could be expected: the presence of a maximum in the flow speed in the centre separates two regions of opposite shear and helps states to be localised close to one side of the channel. Then their dynamics is similar to that in other shear flows, and in particular similar to the one in the ASBL. The fact that the surprising richness in spanwise localised states that show complex sequences of discrete jumps in the spanwise position is found not only in ASBL but also here in plane Poiseuille

flow suggests that there should be a robust mechanism for this dynamics that does not depend on the specific details of the flow. Perhaps the one feature that could be important is the combination between a rigid wall and a softer upper boundary where the shear vanishes: this is the case at the midplane in plane Poiseuille flow and at the upper end of the boundary layer in the ASBL.

The similarity between the dynamics found here in the plane Poiseuille flow and the previous results for the ASBL raises the question to which extent they can be connected. For this one can look for homotopies that transform one flow into the other. Kreilos et al. (2013) show how ASBL and plane Couette can be connected and how the periodic solution appears in a SNIPER-bifurcation of the continuation of a simple equilibrium solution on the way from PCF to ASBL. Waleffe (2003) uses a homotopy between PPF and PCF to relate travelling waves and steady states. So one can expect that a combination of both homotopies can provide a connection between the ASBL and plane Poiseuille flow, but we did not pursue this further.

Several directions for further investigation are evident. It would be most interesting to continue some of these states to the saddle-node bifurcation points so that the upper branch can be identified and one can see how they impact the scaffold for turbulent dynamics (along the lines discussed by Kreilos & Eckhardt (2012) and Avila et al. (2013)). Similarly, it would be interesting to track them with a Newton method and to trace the orbits without the need for edge tracking, so that one can follow the states that branch off at bifurcations. That, however, is challenging and computationally expensive because of the long periods of the orbits which require multi-point shooting methods (Sánchez & Net 2010).

Acknowledgements

We thank Tobias Kreilos for discussions, and John Gibson for providing *Channelflow*. This work was supported by the Deutsche Forschungsgemeinschaft.

References

- Avila M, Mellibovsky F, Roland N & Hof B 2013 *Phys. Rev. Lett.* **110**(22), 224502.
 Cherubini S, De Palma P, Robinet J C & Bottaro A 2011 *Phys. Fluids* **23**(5), 051705.
 Cherubini S, De Palma P, Robinet J C & Bottaro A 2012 *Fluid Dyn. Res.* **44**(3), 031404.
 Clever R M & Busse F H 1997 *J. Fluid Mech.* **344**, 137–153.
 Dijkstra H, Wubs F W, Cliffe A K, Doedel E, Dragomirescu I F, Eckhardt B, Gelfgat A Y, Hazel A L, Lucarini V, Salinger A G, Phipps E T, Sanchez-Umbria J, Schuttelaars H, Tuckerman L S & Thiele U 2014 *Commun. Comput. Phys.* **15**(1), 1–45.
 Duguet Y, Schlatter P & Henningson D S 2009 *Phys. Fluids* **21**(11), 111701.
 Duguet Y, Schlatter P, Henningson D S & Eckhardt B 2012 *Phys. Rev. Lett.* **108**(4), 044501.
 Duguet Y, Willis A P & Kerswell R R 2008 *J. Fluid Mech.* **613**, 255–274.
 Eckhardt B, Faisst H, Schmiegel A & Schneider T M 2008 *Phil Trans R Soc A* **366**, 1297–1315.
 Eckhardt B, Schneider T M, Hof B & Westerweel J 2007 *Annu. Rev. Fluid Mech.* **39**(1), 447–468.
 Ehrenstein U & Koch W 1991 *J. Fluid Mech.* **228**, 111–148.
 Faisst H & Eckhardt B 2003 *Phys. Rev. Lett.* **91**(22), 224502.

- Gibson J F 2012 *Channelflow: A spectral Navier-Stokes simulator in C++* Technical report U. New Hampshire.
- URL:** *Channelflow.org*
- Gibson J F & Brand E W 2014 *J. Fluid Mech.* **745**, 25–61.
- Gibson J F, Halcrow J & Cvitanović P 2009 *J. Fluid Mech.* **638**, 243.
- Hof B, Westerweel J, Schneider T M & Eckhardt B 2006 *Nature* **443**(7107), 59–62.
- Itano T & Generalis S 2009 *Phys. Rev. Lett.* **102**(11), 114501.
- Itano T & Toh S 2001 *J. Phys. Soc. Japan* **70**(3), 703–716.
- Kawahara G & Kida S 2001 *J. Fluid Mech.* **449**, 291.
- Kawahara G, Uhlmann M & van Veen L 2012 *Annu. Rev. Fluid Mech.* **44**(1), 203–225.
- Khapko T, Duguet Y, Kreilos T, Schlatter P, Eckhardt B & Henningson D S 2013 *arXiv Prepr. arXiv1308.5531* pp. 1–11.
- Khapko T, Kreilos T, Schlatter P, Duguet Y, Eckhardt B & Henningson D S 2013 *J. Fluid Mech.* **717**, R6.
- Kreilos T & Eckhardt B 2012 *Chaos* **22**(4), 047505.
- Kreilos T & Eckhardt B 2013 *arXiv Prepr. arXiv1309.4590v1* pp. 1–10.
- Kreilos T, Veble G, Schneider T M & Eckhardt B 2013 *J. Fluid Mech.* **726**, 100–122.
- Mellibovsky F & Eckhardt B 2012 *J. Fluid Mech.* **709**, 149–190.
- Mellibovsky F, Meseguer A, Schneider T & Eckhardt B 2009 *Phys. Rev. Lett.* **103**(5), 054502.
- Melnikov K, Kreilos T & Eckhardt B 2013 *arXiv Prepr. arXiv1309.6912v1* pp. 1–8.
- Nagata M 1990 *J. Fluid Mech* **217**, 519–527.
- Nagata M & Deguchi K 2013 *J. Fluid Mech* **735**, R4.
- Orszag S A 1971 *J. Fluid Mech.* **50**, 689–703.
- Pringle C & Kerswell R R 2007 *Phys. Rev. Lett.* **99**(7), 074502.
- Sánchez J & Net M 2010 *Int. J. Bifurcat. Chaos* **20**(01), 43–61.
- Schneider T M, Eckhardt B & Yorke J 2007 *Phys. Rev. Lett.* **99**(3), 034502.
- Schneider T M, Gibson J F & Burke J 2010 *Phys. Rev. Lett.* **104**(10), 104501.
- Schneider T M, Gibson J F, Lagha M, De Lillo F & Eckhardt B 2008 *Phys. Rev. E* **78**(3), 037301.
- Schneider T M, Marinc D & Eckhardt B 2010 *J. Fluid Mech.* **646**, 441.
- Skufca J, Yorke J & Eckhardt B 2006 *Phys. Rev. Lett.* **96**(17), 174101.
- Strogatz S H 1994 *Nonlinear dynamics and chaos: with applications to physics, biology, chemistry and engineering* Perseus.
- Toh S & Itano T 1999 *arXiv Prepr. physics/9905012* pp. 0–4.
- Toh S & Itano T 2003 *J. Fluid Mech.* **481**, 67–76.
- Tuckerman L & Barkley D 1988 *Phys. Rev. Lett.* **61**(4), 408.
- Uhlmann M, Kawahara G & Pinelli A 2010 *Phys. Fluids* **22**(8), 084102.
- Vollmer J, Schneider T M & Eckhardt B 2009 *New J. Phys.* **11**(1), 013040.
- Waleffe F 1997 *Phys. Fluids* **9**(4), 883.
- Waleffe F 1998 *Phys. Rev. Lett.* **81**(19), 4140.
- Waleffe F 2003 *Phys. Fluids* **15**(6), 1517.
- Wedin H & Kerswell R R 2004 *J. Fluid Mech.* **508**, 333–371.